

# The Effect of Irradiation on the Magnetic Properties of Rock and Synthetic Samples: Implications to Irradiation of Extraterrestrial Materials in Space<sup>1</sup>

N. S. Bezaeva<sup>a, b, c\*</sup>, J. Gattacceca<sup>a, d</sup>, P. Rochette<sup>a</sup>, J. Duprat<sup>e</sup>, G. Rizza<sup>f</sup>,  
P. Vernazza<sup>g</sup>, V. I. Trukhin<sup>h</sup>, and A. Ya. Skripnik<sup>i</sup>

<sup>a</sup> CEREGE CNRS/ Aix-Marseille Université, UM34, 13545 Aix-en-Provence, France

<sup>b</sup> Ural Federal University, ul. Mira 19, Ekaterinburg, 620002 Russia

<sup>c</sup> Kazan Federal University, ul. Kremlyovskaya 18, Kazan, 420008 Russia

<sup>d</sup> Department of Earth, Atmospheric, and Planetary Sciences, Massachusetts Institute of Technology, 7 Massachusetts Avenue, Cambridge, MA 02139, USA

<sup>e</sup> Centre de Spectrométrie Nucléaire et de Spectrométrie de Masse, Bat. 104, 91405 Orsay Campus, France

<sup>f</sup> Laboratoire des Solides Irradiés, Ecole Polytechnique/ CEA (DSM-DRECAM)/CNRS (UMR 7642), 91128 Palaiseau, Cedex, France

<sup>g</sup> Laboratoire d'Astrophysique de Marseille, 38 rue Frédéric Joliot-Curie, 13388 Marseille, France

<sup>h</sup> Earth Physics Department, Faculty of Physics, Lomonosov Moscow State University, Leninskie gory, Moscow, 119991 Russia

<sup>i</sup> Vernadsky Institute of Geochemistry and Analytical Chemistry, Russian Academy of Sciences, ul. Kosygin 19, Moscow, 119991 Russia

\*e-mail: bezaeva@physics.msu.ru

Received November 20, 2013

**Abstract**—We report here the results of laboratory analog experiments to consider the potential effects of solar energetic particles (SEP or solar-flare-associated particles) and galactic cosmic rays (GCR) on the magnetic properties of extraterrestrial materials. We carried out proton bombardment experiments (with irradiation energies  $E_1=400$ ,  $E_2=850$  keV and three irradiation fluences in  $10^{14}$ – $10^{16}$  p/cm<sup>2</sup> range) and lead-ion bombardment experiments ( $E=1$  GeV) on (previously demagnetized by 120 mT alternating magnetic field) rock and synthetic samples with the following magnetic carriers: metallic iron and nickel iron, Ti-rich and Ti-free magnetite, pyrrhotite. Irradiation experiments resulted in either further demagnetization or magnetization of irradiated samples depending on the type of magnetic mineralogy and type of ionizing radiation involved. Apart for the formation of radiation-induced remanent magnetization (RIRM), we observed major changes in bulk magnetic properties, i.e., a moderate to dramatic decrease (up to 93%) in the coercivity of remanence  $B_{cr}$  for all iron-bearing phases (iron-in-epoxy and Bensour meteorite samples). Contrary to iron-bearing samples, several magnetite-bearing samples experienced a radiation-induced magnetic hardening (increase in  $B_{cr}$ ). Magnetic hardening was also observed for Ar<sup>2+</sup> ion-irradiated nickel iron-bearing HED meteorites, measured for comparison with the previously stated results. Therefore, the combined effect of SEP with GCR may magnetically soften iron-bearing materials and harden magnetite-bearing materials. In order to answer the question whether RIRM may account for natural remanent magnetization of meteorites and lunar samples, physical mechanism of RIRM formation and potential dependence of RIRM intensity on the background magnetic field present during irradiation event should be investigated.

**Keywords:** irradiation, protons, lead ions, argon ions, rock magnetism, meteorites, extraterrestrial materials

**DOI:** 10.1134/S1069351315020019

## 1. INTRODUCTION

Before reaching the Earth through meteorite falls or sample return, most extraterrestrial materials have been exposed to space radiations at different stages in their history. In the Solar System there are three main

types of particle radiation: large fluxes of low-energy solar wind (SW) particles, smaller fluxes of high-energy galactic-cosmic-ray (GCR) particles (Diehl et al., 2001), and intermittent intense fluxes of solar-flare-associated particles, also called solar cosmic rays or solar energetic particles (SEP) (Heiken et al., 1991; Eugster et al., 2006). The intensity of SEP flux emitted

<sup>1</sup> The article was translated by the authors.

by the sun during irregular solar-flare events is directly related to the 11-year cycles in solar activity. The intensity of GCR flux in the inner solar system varies by a factor of two within an 11-year solar cycle and reaches its maximum during periods of the minimum solar activity as a result of the modulation of the solar cavity.

Space radiations contribute significantly to the evolution of the surfaces of airless bodies in the Solar System. SW ion irradiation modifies the remotely sensed properties of the surfaces of airless Solar System bodies and can impede our ability to remotely assess the mineralogy and other attributes of the surfaces of asteroids and other airless bodies (Vernazza et al., 2008; 2009). The spectral effects due to the continuous bombardment by SW ions have been previously studied through laboratory experiments in order to explain the observed spectral mismatch between lunar soils and underlying rocks, and between the most populous class of meteorites (ordinary chondrites) and the surface spectra of their presumed (*S*-type) asteroidal parent bodies (Pieters et al., 2000; Hapke, 2001; Brunetto and Strazzulla, 2005; Strazzulla et al., 2005; Vernazza et al., 2006). These experiments demonstrate that space weathering processes can be the cause of the observed spectral mismatch.

In this paper, we investigate experimentally the possibility that space radiations affect the magnetic properties of the solid matter in the Solar System. The influence of SW (with typical energies  $E$  about 1 keV/u; where eV/u = electron volts per atomic-mass-unit) on the magnetic properties can be neglected as the associated penetration depth is in the nm-range and its effect on bulk magnetic properties of extraterrestrial materials would not be detectable during experimental simulations in laboratory conditions nor significant in space. So, we will further discuss only SEP and GCR.

Proton-irradiation experiments were used to simulate the lower part of SEP energy spectrum ( $E_p \sim 1$  MeV). Laboratory simulation of GCR irradiation was realized via lead-ion bombardment with  $E = 1$  GeV or  $\sim 5$  MeV/u. Finally, argon-ion irradiation was performed with  $E = 400$  keV (or  $\sim 10$  keV/u). We report the effects of these radiations on the magnetic properties of terrestrial rocks, meteorites and synthetic samples with a variety of magnetic minerals (metallic iron and nickel iron, Ti-rich and Ti-free magnetite, pyrrhotite). This question has previously received only little attention (Butler and Cox, 1971; 1974; Rowe, 1978) in spite of potential important applications in particular for the interpretation of the magnetic properties and the paleomagnetic record of meteorites with implications for the understanding of the evolution of the early Solar System and the evolution of its solid bodies (Rochette et al., 2009a; Weiss et al., 2010).

## 2. STATE-OF-THE ART AND GLOBAL CONTEXT

According to a one-stage irradiation model (e.g., [Herzog, 2005]), while on their parent bodies, meteoroids are shielded from cosmic radiations until fragmentation. Cosmic ray exposure (CRE) ages can be estimated for different types of meteorites from the abundance in meteorites of certain nuclides produced during their interactions with cosmic rays. After fragmentation by impact mechanism and before entering the Earth's atmosphere, meteoroids are directly exposed to SEP and GCR during periods that are typically of several Myr (Sears, 2004). Space radiation fluxes are mostly composed by protons ( $p$ ) and He/ $p$  (with a typical He/ $p$  ratio of  $\sim 0.1$  for GCR and  $\sim 0.02$  for SEP (Kapitonov, 2002)). A lesser flux of heavier ions (atomic number  $Z \geq 6$ ) accounts for  $\sim 1\%$  of GCR [Kapitonov, 2002].

The present-day proton flux intensities (fluences  $\phi$ ) are  $\phi_{\text{SEP}} \sim 100 p/\text{cm}^2 \text{ s}$  (for  $E > 10$  MeV protons) for SEP and  $\phi_{\text{GCR}} \sim 3 p/\text{cm}^2 \text{ s}$  for GCR [Heiken et al., 1991]. The penetration depth in the solid matter varies from  $\mu\text{m}$  to mm for SEP protons (with  $E$  from  $\sim 1$  MeV/u up to tens MeV/u) up to cm for GCR heavy ions and cm to meters for GCR protons (with  $E$  from 0.1 to  $> 10$  GeV/u). Interaction of GCR nuclei with solid matter induces nuclear reactions in material accompanied by a production of secondary neutrons.

Previous works showed that neutron bombardment can result in magnetic ordering of iron-nickel single crystals (Néel et al., 1964) and magnetic hardening of kamacite (body-centered cubic ( $B_{cc}$ ) metallic iron nickel alloy with less than 5–6 wt % Ni) and iron (Butler and Cox, 1971; 1974). However, because the cross-section of nuclear reactions—source of secondary neutrons—is small, this process has little effect in meteorites (Eugster et al., 2006).

It is known that the recovered mass of meteorites is much smaller than a mass of the corresponding pre-atmospheric meteoroids due to ablation and fragmentation processes during Earth's atmospheric entry (e.g., (Bronshen, 1983)). Ablation ( $A$ ) is a loss of mass resulting from the melting of the outer layer and the successive liquid film blowing by an incident air flow, as well as evaporation of the substance and its removal in form of vapors [Bronshen, 1983].  $A$  can be presented as following:

$$A(\%) = (1 - m/M) \times 100, \quad (1)$$

where  $m$  is fallen (collected) mass of meteorite and  $M$  is pre-atmospheric mass of meteoroid. Ablation efficiency mainly depends on  $M$  and pre-atmospheric velocity  $V_e$  of meteoroid ( $V_e \in [11.2; 72.8]$  km/s but practically  $V_e \leq 30$  km/s (Ceplecha et al., 1998)) as well as its shape and the velocity at the trajectory point where ablation ceases and meteoroid passes to dark-flight with velocity approaching gradually to free fall regime (Ceplecha et al., 1998). There are numerous

estimations of  $A$  for different types of meteorites. For example, according to Alexeev (2003; 2004), mean  $A$  for chondrites is  $91.5_{-2.6}^{+2.1}\%$  (found for 262 chondrites) and for ordinary chondrites (OC) is  $78.4_{-3.4}^{+3.1}\%$  (found for 83 OC).

Thus, any traces of the effects of irradiation on the meteoroid surface during the transfer to Earth are lost during atmospheric entry due to dramatic meteoroid mass loss. However, the effect of irradiation by SEP (MeV protons, penetrating up to hundreds of  $\mu\text{m}$  or even up to cm for the most energetic) on the magnetic properties is likely to be detectable on the surfaces of the solid Solar System bodies, as well as in micrometeorites and extraterrestrial materials originating from regolith (lunar meteorites, lunar samples, regolith breccias meteorites [Bischoff et al., 2006]).

Moreover, at an early stage of their evolution, primordial extraterrestrial materials in form of dust in the protoplanetary disk before accretion were directly exposed to possibly intense space radiations. The survey of pre-main-sequence stars with masses ranging from 0.4 to 2 solar mass by the Chandra Orion Ultradeep Project (Wolk et al., 2005) indicates that for these young stellar objects the hard X-ray luminosity  $L$  is ranging from  $10^{30}$  to  $10^{31}$   $\text{erg s}^{-1}$  (Preibisch and Feigelson, 2005). Using an analogy with impulsive flares observed in the contemporary Sun, Lee et al. (1998) obtained a scaling factor between  $L$  and the kinetic energy contained in protons with energies above 10 MeV. One can then estimate that SEP flux suffered by solids at the vicinity of the proto-sun during the first Myrs was  $10^5$  times higher comparing to the present-day SEP flux (Feigelson et al., 2002; Goswami et al., 2001), i.e., in the  $10^7$   $p/\text{cm}^2$  s range.

Changes in natural remanent magnetization (NRM) may represent one of important consequences of irradiation of extraterrestrial materials in space. The question on the possibility of formation of radiation-induced remanent magnetization (RIRM) was first put forward in the work (Rowe, 1978), however to present the RIRM hypothesis has never been confirmed experimentally. In our work this hypothesis was tested for the cases of proton- and lead-ion-bombardments.

### 3. MATERIALS AND METHODS

#### 3.1. Description of Samples

Proton and ion irradiation experiments were carried out on ten different samples (each giving several sister subsamples, see Table 1) with the following magnetic carriers: magnetite ( $\text{Fe}_3\text{O}_4$ ) and titanomagnetite ( $\text{Fe}_{3-x}\text{Ti}_x\text{O}_4$ ), iron ( $\alpha\text{-Fe}_0$ ) and nickel iron ( $\text{FeNi}$ ), and pyrrhotite ( $\text{Fe}_{1-x}\text{S}$ ). These samples consist of two terrestrial rocks, one pure mineral, four samples of dispersed powders (synthetic iron and magnetite, natural monoclinic pyrrhotite) in epoxy resin, and three meteorites.

The two rock samples are a magnetite-bearing microdiorite described by Gattacceca et al. (2007) and a titanomagnetite-bearing basalt described by Gattacceca et al. (2008a). The pure mineral phase consists of monocrystals of hexagonal pyrrhotite (with a small admixture of monoclinic pyrrhotite)<sup>2</sup> described in (Carpenter, 1974; Rochette et al., 2003a). The two powdered samples are powdered natural monoclinic pyrrhotite uniformly dispersed in epoxy resin, with grain sizes in the range 150–250  $\mu\text{m}$  and 75–100  $\mu\text{m}$ , hereafter named monoclinic pyrrhotite 1 and 2, respectively (see Table 1). The original sample—source of pyrrhotite powder, is described by Dekkers (1988). The other two powdered samples are synthetic samples of iron with grain size 10  $\mu\text{m}$  and magnetite with grain size <25  $\mu\text{m}$ , which were prepared using commercial synthetic powders that were dispersed in epoxy. The studied meteorites are Bensour (LL6 ordinary chondrite), Bereba (eucrite) and Tatahouine (diogenite). The last two meteorites are achondritic meteorites from the HED (Howardite-Eucrite-Diogenite) clan, whose parent body is supposed to be asteroid Vesta (Consolmagno and Drake, 1977; Binzel and Xu, 1993). The magnetic properties of Bensour are dominated by tetrataenite [Gattacceca et al., 2003]. However, the Bensour sample was heated up to 650°C under argon atmosphere prior to irradiation experiments, to transform tetrataenite in taenite (face-centered cubic (fcc) metallic nickel iron with  $\text{Ni} \geq 7\%$ , which occurs in many types of meteorites (Sugiura et al., 1988; Rochette et al., 2003b; 2008; 2009b)). Bereba and Tatahouine magnetic mineralogy is dominated by Ni-poor nickel iron in form of kamacite (Rochette et al., 2009b).

The samples of basalt used in proton irradiation experiments, were obtained from a standard thin section (30  $\mu\text{m}$  in thickness). The other samples were 20 to 50  $\mu\text{m}$  in thickness and were glued on top of epoxy disks for easier manipulation (Fig. 1). For lead-ion irradiation, the thickness of samples was 300  $\mu\text{m}$ . All samples were prepared using a diamond wire saw and then abrasive papers for further manual polishing. Main bulk rock magnetic properties of investigated samples before irradiation are presented in Table 1.

Samples were numbered from 1 to 8 (each number corresponding to a given lithology or mineralogy). For proton irradiation, three total fluences  $\phi$  ( $\phi_1 < \phi_2 < \phi_3$ ) were used on three identical groups of samples, spanning three orders of magnitude from  $\phi_1 = 1.2 \times 10^{14}$  to  $\phi_3 = 10^{16}$   $p/\text{cm}^2$  (see below, part 3.2). Names of corresponding samples are composed by the sample number (from 1 to 8) followed by “1” for  $\phi_1$ , “2” for  $\phi_2$  and “3” for  $\phi_3$  (see Table 1 and Fig. 1). Only one fluence was used for lead-ion irradiation experiment. For these samples irradiated with the ions, sample numbers are followed by “a” (and “b” when two samples

<sup>2</sup> This sample is called “hexagonal pyrrhotite” further in the text for brevity.

**Table 1.** Main bulk rock magnetic properties of samples before proton and lead-ion bombardments.

Sample (magnetic carrier)	$\chi_0$	$SIRM$	$MDF_i$	$B_c$	$B_{cr}$	$B_{cr}/B_c$	$M_s$	$M_{rs}/M_s$
Sample ID								
<i>Microdiorite (magnetite)</i>								
1-1	274	0.75	9	2	24	12.0	34.6	0.02
1-2	257	0.83	8	3	28	9.3	33.8	0.02
1-3	117	0.45	9	3	34	11.3	17.6	0.02
1-a	782	1.77	8	2	17	8.5	90.9	0.01
<i>Basalt (titanomagnetite)</i>								
2-1	50.7	1.37	10	10	21	2.1	3.7	0.23
2-2	54.2	1.20	9	9	16	1.8	2.7	0.24
2-3	66.1	1.80	10	11	20	1.8	3.6	0.27
2-a	761	8.22	9	5	14	2.8	47.2	0.13
<i>Hexagonal pyrrhotite</i>								
3-1	12.9	2.77	>150	217	–	–	1.3	0.48
3-2	9.2	1.83	>150	344	294	0.9	0.8	0.65
3-3	12.6	2.63	>150	152	–	–	2.3	0.31
3-a	18.6	4.31	>150	226	–	–	1.8	0.46
3-b	16.7	4.31	>150	184	166	0.9	2.2	0.52
<i>Monoclinic pyrrhotite 1</i>								
4-1	32.0	1.56	9	11	20	1.8	5.9	0.23
4-2	28.4	1.63	8	12	21	1.8	5.5	0.23
4-3	25.3	1.64	8	12	22	1.8	4.8	0.23
4-a	67.7	3.90	8	10	16	1.6	13.5	0.26
<i>Monoclinic pyrrhotite 2</i>								
5-1	28.9	2.71	13	16	25	1.6	7.3	0.34
5-2	24.0	2.41	12	18	27	1.5	6.3	0.34
5-3	32.2	3.13	11	16	24	1.5	8.1	0.35
5-a	44.6	5.25	12	15	22	1.5	12.3	0.37
<i>Iron-in-epoxy</i>								
6-1	47.3	0.07	13	2	30	15.0	11.2	0.01
6-2	50.9	0.08	13	1	62	62.0	13.0	0.003
6-3	57.7	0.07	13	1	28	28.0	14.5	0.003
6-a	134	0.16	9	2	12	6.0	29.8	0.01
6-b	102	0.13	10	2	13	6.5	23.5	0.01
<i>Bensour meteorite (FeNi)</i>								
7-1	3.7	0.04	17	6	56	9.3	1.2	0.02
7-2	3.9	0.04	11	5	50	10.0	1.4	0.02
7-3	34.1	0.15	5	3	55	18.3	10.2	0.01
7-a	190	0.21	16	1	30	30.0	63.2	0.003
<i>Magnetite-in-epoxy</i>								
8-1	4.9	0.11	18	14	32	2.3	0.7	0.14
8-2	7.5	0.14	17	12	34	2.8	1.1	0.10
8-3	14.1	0.22	16	11	24	2.2	1.9	0.10
8-a	42.1	0.57	15	10	25	2.5	5.8	0.09

$\chi_0$  is low field magnetic susceptibility (in  $\times 10^{-12} \text{ m}^3$ );  $SIRM$  is a 3 T isothermal remanent magnetization (in  $\text{Am}^2$ ) measured with a 2G SQUID magnetometer;  $MDF_i$  is median destructive field of  $SIRM$  (in mT);  $B_c$  and  $B_{cr}$  are coercivity and coercivity of remanence (in mT), respectively;  $M_s$  and  $M_{rs}$  are induced saturation magnetization and saturation remanent magnetization (in  $\text{Am}^2$ ), respectively.

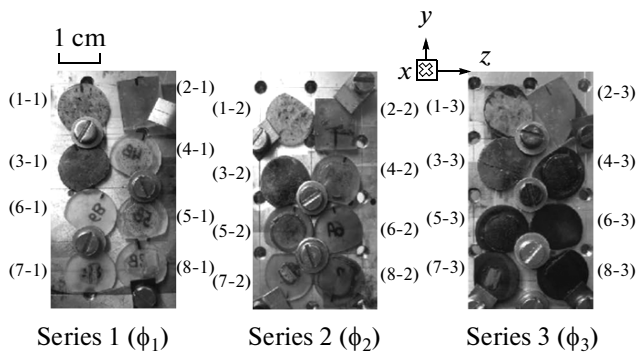


**Fig. 1.** Photograph of proton-irradiated samples inside ARAMIS accelerator after the end of proton bombardment. All samples are indicated by numbers. Conformity of sample numbers to concrete samples is presented in Table 1.  $\{x, y, z\}$  is coordinate system of 2G SQUID magnetometer.

were irradiated). Three additional bulk subsamples were prepared for additional experiments (see below): iron subsample 6-4 and hexagonal pyrrhotite subsamples 3-4 ( $m = 36.5$  mg) and 3-5 ( $m = 21.7$  mg).

Argon-ion ( $\text{Ar}^{2+}$ ) irradiation experiments were conducted only on Bereba and Tatahouine meteorite samples. The experimental procedure is described in Fulvio et al. (2012) and Vernazza et al. (2006). Both samples were in form of pellets, obtained by pressing (2 tons for 5–10 s) the original meteorite powder with grain size in the 10–100  $\mu\text{m}$  range on top of a non-magnetic (KBr) support disk. We studied the magnetic properties of nine pristine (i.e., non-irradiated) bulk samples of Tatahouine to check the level of homogeneity of the original magnetic properties at the scale of studied samples  $\sim 0.1$  g. One pristine pellet of Bereba meteorite was also studied.

### 3.2. Methodology of Irradiation Experiments

Irradiation by protons was performed with the ARAMIS accelerator (Bernas et al., 1992) part of the JANNuS facility (Serruys et al., 2005) at the Centre de Spectrométrie Nucléaire et de Spectrométrie de Masse (CSNSM, Orsay, France). We used three identical groups of samples that we irradiated using the following total proton fluences:  $\phi_1 = 1.2 \times 10^{14}$   $p/\text{cm}^2$ ,  $\phi_2 = 1.2 \times 10^{15}$   $p/\text{cm}^2$  and  $\phi_3 = 10^{16}$   $p/\text{cm}^2$ . The typical beam intensity was  $I_p = 1\text{--}3$   $\mu\text{A}$  (under vacuum  $< 4 \times 10^{-6}$  mbar) and the exposure time varied from a few minutes for minimum irradiation fluence ( $\phi_1$ ) to a few hours for maximum irradiation fluence ( $\phi_3$ ).<sup>3</sup> All sam-

<sup>3</sup> Magnetic field strength  $B$  was not measured during proton bombardment. Static magnetic field inside accelerator on the samples' level, measured after the end of irradiation experiments at ambient pressure and room temperature using fluxgate magnetometer MAG-01 (by Bartington Instruments with sensitivity of 1 nT) is  $B = 146$   $\mu\text{T}$ .

ples were carbon-coated ( $15 \pm 1$  nm) prior to proton bombardment. Based on the values of irradiation energies and material densities, the maximum penetration depth of protons into the samples was estimated as 15–20  $\mu\text{m}$  using SRIM software [Ziegler, 2004]. In order to have different penetration depths and thus magnify possible radiation-induced changes, we irradiated all samples with the above indicated fluences twice: with irradiation energies  $E_1 = 400$  keV and  $E_2 = 850$  keV, respectively. Proton fluxes with such energies do not induce nuclear reactions within irradiated samples. It is important to emphasize that all samples were thicker than estimated maximum proton penetration depth (25–50  $\mu\text{m}$  against 15–20  $\mu\text{m}$ ), so that proton bombardment resulted in implantation of protons into the target material.

Irradiation by lead ions was performed at Grand Accélérateur National d'Ions Lourds (GANIL, Caen, France) with  $E = 1$  GeV (or  $\sim 5$  MeV/u). Corresponding maximum penetration depth was estimated as 200  $\mu\text{m}$  using SRIM software [Ziegler, 2004]. All samples were covered by aluminum foil prior to lead ion bombardment. Neither mechanical destruction, nor loss of mass, were observed on the samples after proton and ion bombardment (see Table 2).

Irradiation of samples by argon ions  $\text{Ar}^{2+}$  was previously performed at the Observatory of Catania (Italy) by Vernazza et al. (see Vernazza et al., 2006) for the description of experimental setup).  $\text{Ar}^{2+}$  fluence and energy were of  $6.6 \times 10^{15}$   $\text{Ar}^{2+}/\text{cm}^2$  and 400 keV, respectively. In all experiments the thickness of samples was greater than estimated proton or ion penetration depth. Thus, bombardment particles remained implanted into the target materials.

### 3.3. Methodology of Magnetic Measurements

All magnetic measurements were performed at CEREGE (Aix-en-Provence, France). For irradiation experiments with protons and lead ions, pre-irradiation and post-irradiation magnetic analyses were carried out on the same samples. For samples irradiated with argon ions, magnetic analyses were carried out on irradiated samples and other pristine samples of the same meteorites for comparison.

The standard sequence of magnetic measurements, performed twice (before and after irradiation experiments), is presented below. Natural remanent magnetization or post-irradiation remanence was measured and samples were demagnetized stepwise by alternating magnetic field (AF) up to 150 mT using 2G Enterprises SQUID magnetometer equipped with online AF demagnetizer and allowing the measurement of magnetic moment up to  $10^{-4}$   $\text{Am}^2$  with a noise level of  $10^{-11}$   $\text{Am}^2$ . Room temperature hysteresis loops measurements were performed using a Princeton Micro-mag Vibrating Sample Magnetometer (VSM) with maximum applied magnetic field of 1T and sensitivity of  $\sim 10^{-9}$   $\text{Am}^2$ . The analysis of hysteresis loops pro-

**Table 2.** Relative changes in bulk rock magnetic properties of samples after proton and lead-ion bombardments

Sample (magnetic carrier)	$\Delta m$	$\Delta\chi_0$	$\Delta SIRM$	$\Delta MDF_i$	$\Delta B_c$	$\Delta B_{cr}$	$\Delta M_s$
Sample ID							
<i>Microdiorite (magnetite)</i>							
1-1	0.1	1	-2	-1	3	15	9
1-2	0.0	1	-3	-5	-9	-1	5
1-3	0.2	2	-6	-5	2	-11	1
1-a	—	-6	8	4	25	17	-4
<i>Basalt (titanomagnetite)</i>							
2-1	0.1	-4	-11	0	-1	-4	-4
2-2	0.2	-4	-21	-5	-1	0	36
2-3	0.0	-2	-20	-2	-7	-1	-5
2-a	—	-15	-6	-6	4	-3	-2
<i>Hexagonal pyrrhotite</i>							
3-1	0.1	-3	-16	—*	0	—	9
3-2	0.0	-5	-19	—*	5	-17	9
3-3	0.4	-4	-9	—*	4	—	-1
3-a	—	15	6	—**	-25	—	-5
3-b	—	6	-1	—**	-12	3	0
<i>Monoclinic pyrrhotite 1</i>							
4-1	0.2	-2	1	-7	2	2	-3
4-2	0.1	1	2	1	-2	-3	22
4-3	0.4	-5	2	0	0	-2	-4
4-a	—	13	-6	-4	0	2	-2
<i>Monoclinic pyrrhotite 2</i>							
5-1	0.1	-5	1	2	3	-1	-16
5-2	0.2	-6	0	-1	0	-5	-16
5-3	0.5	4	0	1	-1	-2	-2
5-a	—	19	-12	-3	-2	0	10
<i>Iron-in-epox</i>							
6-1	0.1	1	-20	-24	-27	-76	3
6-2	0.0	-1	-17	-17	-29	-90	-5
6-3	0.8	-2	-23	-23	-29	-63	-3
6-a	—	-3	14	4	2	-58	11
6-b	—	-3	3	0	-12	-2	12
<i>Bensour meteorite (Ni-Fe)</i>							
7-1	0.1	16	-16	-29	40	-53	-1
7-2	0.1	-7	-34	-19	-6	-93	-2
7-3	0.1	-1	-7	-4	10	-66	3
7-a	—	0.2	37	-15	25	-6	-2
<i>Magnetite-in-epoxy</i>							
8-1	0.0	-8	-20	-13	-9	-4	-7
8-2	0.6	-38	30	15	-3	-8	-22
8-3	0.7	3	-16	-13	-6	23	-19
8-a	—	-29	-16	9	11	21	-33

All values are in %. Relative changes were calculated for each parameter  $A$  using the following equation:  $\Delta A = (A_2 - A_1)/A_1 \times 100\%$ , where  $A_1$  and  $A_2$  are the corresponding pre- and post-irradiation values, respectively. Thus, negative and positive  $\Delta A$  indicate proton-irradiation induced decrease and increase in the corresponding value  $A$ , respectively.  $m$  is sample mass;  $\chi_0$  is low field magnetic susceptibility;  $SIRM$  is a 3 T isothermal remanent magnetization (in  $\text{Am}^2$ ) measured with a *2G SQUID* magnetometer;  $MDF_i$  is median destructive field of  $SIRM$ ;  $B_c$  and  $B_{cr}$  are coercivity and coercivity of remanence, respectively;  $M_s$  and  $M_{rs}$  are induced saturation magnetization and saturation remanent magnetization, respectively.

\* Post-irradiation  $MDF_i$  was within [147, 150] mT range and pre-irradiation  $MDF_i$  was > 150 mT.

\*\* Pre- and post-irradiation  $MDF_i$  > 150 mT.

vided saturation remanent magnetization ( $M_{rs}$ ), saturation magnetization ( $M_s$ ) and the coercivity ( $B_c$ ). Remanent coercivity ( $B_{cr}$ ) was determined by DC (direct current) backfield remanence demagnetization experiments performed with the VSM. Measurements of low field magnetic susceptibility  $\chi_0$  were performed with KLY2 and MFK1 apparatus from Agico. Each sample was imparted a saturation isothermal remanent magnetization (SIRM) in a 3 T magnetic field using a pulse magnetizer MMPM9 (by Magnetic Measurements). Finally, SIRM was measured and stepwise demagnetized by AF up to 150 mT. The residual remanent magnetization before irradiation experiments is denoted as  $I_{r0}$  in the following (in case of proton bombardment  $I_{r0}$  corresponds to remanent magnetization, remained after one extra step—new formation of SIRM and its one-step AF demagnetization by 120 mT). Orientation of the samples was kept throughout the experiments (see Fig. 1) in order to test the concept of RIRM, previously put forward by Rowe (1978). It was tested for both proton and lead-ion bombardments.

### 3.4. Basic Principles of Interaction of Ionizing Radiation with Solid Matter

For better understanding of experimental results presented below (see parts 4.2–4.4), we will briefly treat here some basic physical principles for interaction of ion beam with target materials in case of metals (proton being considered as the lightest ion). As mentioned in introduction, for both proton and lead-ion irradiation experiments the irradiation energies were chosen to be lower than the corresponding nuclear reaction barriers. That is why the ion beam interacts with target materials only via (1) direct ionization of a target material or (2) elastic collisions with the lattice atoms of the target, or both [Holbert, 2008]. Charged particles lose their kinetic energy almost entirely through ionization of the target until their energy drops below a threshold level  $E_{th}$ , which is about 1 keV for metallic iron (Butler and Cox, 1971). However, there is no permanent damage from ionization in metals (with their shared electrons) and the mechanism (2) is the radiation damage mechanism of importance (Holbert, 2008). Below  $E_{th}$  bombarding particles lose their energy via atomic displacement, resulting in creation of point defects (such as a vacancy and an interstitial atom) in the crystalline structure. A single incident particle can cause a “collision cascade”, when the primary displaced atom (primary “knock-on”) will further displace other lattice atoms (Butler and Cox, 1971; 1974).

According to the basic theory on radiation damage in metallic solids, summarized e.g., by Butler and Cox [1974], the energy, which the primary “knock-on” may receive, is limited and given by:

$$E_p(Max) = 4EMm/(M + m)^2, \quad (2)$$

where  $E$  and  $M$  are energy and mass of incident particle, respectively;  $m$  is mass of lattice atom.

The average energy received by the primary “knock-on” is given by:

$$\bar{E}_p = E_d \ln\left(\frac{E_p(Max)}{E_d}\right), \quad (3)$$

where  $E_d$ —energy required to displace an atom from its lattice site ( $E_d \sim 27$  eV for metallic iron (Dienes and Vineyard, 1957)).

For  $E_p \gg E_d$  (our case), average number of displaced atoms per primary collision is:

$$\tilde{\nu} \cong \frac{\bar{E}_p}{2E_d}. \quad (4)$$

Thus, in case of iron target, proton bombardment resulted in the “collision cascades” of  $\tilde{\nu} \sim 3.5$  ( $\bar{E}_p = 187$  eV) and  $\tilde{\nu} \sim 3.9$  ( $\bar{E}_p = 208$  eV) displaced atoms of Fe per primary collision for  $E_1 = 400$  keV and  $E_2 = 850$  keV protons, respectively. For 1 GeV lead-ion bombardment,  $\tilde{\nu} \sim 8.5$  ( $\bar{E}_p = 459$  eV).

Accumulation of point defects above certain critical concentration (critical displacement damage) may result in partial atom disorder or amorphization (i.e., crystal-to-amorphous transformation) of irradiated zone during ion implantation (e.g., Tetelbaum and Mendeleva [2004], the authors suggest a simple mechanical model of amorphization of solids). Microstructural changes in irradiated solids may then affect their macroscopic properties such as bulk magnetic properties.

Amorphization of solids by fast neutrons ( $\phi \sim 10^{20} \text{ cm}^{-2}$ ) was reported in many papers (e.g., (Dubinin et al., 1998)), some solids do not show any amorphization by fast neutrons but simple atom disorder (Dubinin et al., 1998). Irradiation ordering—the effect opposite to amorphization—was reported by Néel et al. (1964) for iron-nickel single crystal after neutron bombardment. Please note that the above-mentioned mechanism of mechanical amorphization is fundamentally temperature-independent and is totally different from amorphization effect associated with local melting along ion (or neutron) tracks and further rapid cooling, which results in solidification of amorphous phase inside irradiated solids (Tetelbaum and Mendeleva, 2004).

It is interesting to mention that ion irradiation can be a source of impurity production in crystalline lattice (Holbert, 2008). Indeed, bombarding protons slow down and capture necessary electrons to render them neutral. So, the proton becomes hydrogen and may cause swelling in the material by internal pressurization of neighboring atoms (Holbert, 2008). However, no proton-radiation-induced swelling was observed in our samples.

## 4. RESULTS AND DISCUSSION

### 4.1. Irradiation by Protons

**4.1.1. Thermal effects.** Proton-irradiated samples are shown in Fig. 1 (photo). Radiation-induced changes in bulk rock magnetic properties and magnetic remanence are presented in Table 2 and Table 3, respectively.

As one can see from Fig. 1, increasing changes in the color of epoxy are observed with increasing proton fluences. Although temperature control performed with a thermocouple embedded in epoxy during irradiation experiments indicated no heating above 38°C, the observed darkening of epoxy may indicate heating of samples during proton bombardment. In order to estimate a qualitative upper temperature limit, we carried out stepwise heating of epoxy samples up to 230°C. The color of the 1<sup>st</sup> group was reached at 110°C <  $T_1$  < 160°C; the color of the 2<sup>nd</sup> group was reached at  $T_2 \sim 190^\circ\text{C}$ ; the color of the 3<sup>d</sup> group was reached at  $T_3 \sim 230^\circ\text{C}$ . This is in agreement with reports that thermal aging of epoxy resin starts at 120°C, whereas short exposure to 230–250°C causes its destruction (Gordon, 1963). As there was no mechanical destruction of irradiated samples,  $T_3$  did not exceed 230°C.

Contrary to heating experiments, proton bombardment is able to promote epoxy darkening through another physical mechanism. Darkening of organic polymer may take place due to chemical reaction of protons with polymer structure, which results in bond break of polymer molecules and liberation of different elements such as carbon via chain scission reactions [Koptelov et al., 2008]. Indeed, radiation-induced fragilization and carbonization of epoxy resin was reported by Kircher and Bowman (1964). It is interesting to note that Koptelov et al. (2008) stated that changes in physical properties of polymers appears as a result of chain scission reactions below certain critical fluence  $\phi_{cr}$ . Above  $\phi_{cr}$  one may expect a visible loss of dielectric properties under irradiation. Proton critical fluence for the investigated by Koptelov et al. [2008] polymer (Kapton C<sub>22</sub>H<sub>10</sub>N<sub>2</sub>O<sub>5</sub>) was found to be  $\phi_{cr} = 3.1 \times 10^{16}$  p/cm<sup>2</sup>, which is above our maximum proton fluence  $\phi_3$ . Thus, in all our experiments epoxy resin retained its properties of insulator under proton bombardment. As it was used as a nonmagnetic matrix in all our synthetic samples (see Table 1), it could protect magnetic grains from throughout uniform heating due to its low thermal conductivity.

Thus, in our experiments radiation-induced darkening of samples is likely to be due to both carbonization of epoxy and simultaneous heating up to temperatures no higher than  $T_1$ ,  $T_2$ ,  $T_3$  (see above). Possible heating is likely to have been local and having affected only the upper layers of the samples. Heating of samples may result in annealing of some old and newly created crystalline lattice defects, thus making the radiation-induced changes in bulk magnetic proper-

ties less visible. That is why, if not stated otherwise, we will further involve into discussion of irradiation dose dependence of bulk magnetic properties only the samples of groups 1 & 2 and will consider possible heating as an issue for the samples of group 3. It is important to mention that the only samples with Curie temperatures below 200°C were basaltic samples ( $T_c = 150^\circ\text{C}$ ), all other samples had much higher Curie temperatures (295°C for hexagonal pyrrhotite, 325°C for monoclinic pyrrhotite samples, and above for other samples), which excludes a possibility of acquisition of significant thermo-remanent magnetization due to heating of the samples and subsequent cooling in the magnetic field of irradiation zone<sup>3</sup>.

**4.1.2. Radiation-induced changes in bulk magnetic properties of samples.** Relative changes (in %) in bulk magnetic properties upon proton irradiation are presented in Table 2. There is a dramatic decrease (53 to 93%) in  $B_{cr}$  observed for all iron and Bensour meteorite samples.  $B_{cr}$  decreases with increasing  $\phi$  (Fig. 2). Magnetic softening may have resulted from radiation-induced amorphization or atom disorder of iron phases (discussed above), consistent with the observed associated decrease in SIRM (7–34%). All iron-in-epoxy samples also show a decrease in  $B_c$  (27 to 29%) and  $MDF_i$  (17 to 24%) after proton bombardment but negligible changes in  $\chi_0$  ( $\leq 2\%$ ) and  $M_s$  ( $\leq 5\%$ ).

Butler and Cox (1974) previously reported 5–20% increase in  $B_c$  of multidomain iron and kamacite after neutron bombardment ( $B_c$  returned to its pre-irradiation values upon annealing at 200–300°C [Butler and Cox, 1974]). These results are not directly comparable with our experiments due to different nature of bombarding particles (neutral vs charged particles). In addition, there is no information in [Butler and Cox, 1974] on  $B_{cr}$  before and after irradiation for comparison; pre-irradiation  $B_c$  values were within 0.028–0.08 mT range, which is much lower than our pre-irradiation  $B_c$  values (1–2 mT, see Table 1).

In order to ascertain that the observed magnetic softening of iron is not due to possible radiation-induced heating, we carried our supplementary heating experiments on a pristine iron-in-epoxy sample (sample 6-4). A minor decrease in  $B_{cr}$  (from 21 to 19 mT) upon stepwise heating up to 230°C is observed, but cannot account for the changes observed during the irradiation experiment (Fig. 3). Heating of non-irradiated piece of taenite-bearing Bensour meteorite up to 115°C also resulted in a minor change in  $B_{cr}$  (from 33 to 32 mT).

There are no significant radiation-induced changes in  $B_{cr}$ ,  $B_c$  or SIRM observed for the samples of monoclinic pyrrhotite, although  $M_s$  values change up to 22% (both increase and decrease are observed for different samples, see Table 2). Significant increase in  $M_s$  is observed for one basaltic sample (36%), whereas magnetite-in-epoxy samples show an  $M_s$  decrease (7 to 22%).

**Table 3.** Magnetic remanence of the samples before and after proton bombardment

Sample	$I_{rx}$	$I_{ry}$	$I_{rz}$	$I_r$	Sample	$I_{rx}$	$I_{ry}$	$I_{rz}$	$I_r$
Sample ID (**)					Sample ID (**)				
<i>Microdiorite</i>					<i>Monoclinic pyrrhotite 2</i>				
1-1 ( $I_{r0}$ )	0.1	3.1	-0.1	3.1	5-1 ( $I_{r0}$ )	0.2	2.7	-0.1	2.7
1-1 (RIRM)	1.3	3.1	-1.2	3.5	5-1 (RIRM)	3.6	2.2	2.8	5.1
1-2 ( $I_{r0}$ )	-0.2	2.2	-0.2	2.2	5-2 ( $I_{r0}$ )	0.0	3.3	-0.4	3.4
1-2 (RIRM)	-0.1	1.6	1.3	2.1	5-2 (RIRM)	10	-2.2	-1.4	10
1-3 ( $I_{r0}$ )	0.4	3.0	0.2	3.1	5-3 ( $I_{r0}$ )	0.7	3.0	0.1	3.1
1-3 (RIRM)	1.3	3.2	1.9	3.9	5-3 (RIRM)	1.4	2.3	-0.1	2.7
1-a ( $I_{r0}$ )	—	—	—	1.9	5-a ( $I_{r0}$ )	—	—	—	2.6
1-a (RIRM)	-1.2	0.2	4.6	4.8	5-a (RIRM)	-1.7	-0.3	0.1	1.7
<i>Basalt</i>					<i>Iron-in-epoxy</i>				
2-1 ( $I_{r0}$ )	-0.6	5.6	0.0	5.7	6-1 ( $I_{r0}$ )	-0.1	3.8	-0.5	3.8
2-1 (RIRM)	4.4	6.4	2.2	8.0	6-1 (RIRM)	1.9	2.3	-2.4	3.9
2-2 ( $I_{r0}$ )	-0.5	6.1	0.1	6.1	6-2 ( $I_{r0}$ )	-0.1	3.4	0.2	3.4
2-2 (RIRM)	2.4	7.8	1.2	8.2	6-2 (RIRM)	5.1	0.4	1.4	5.3
2-3 ( $I_{r0}$ )	-0.7	6.0	-0.1	6.0	6-3 ( $I_{r0}$ )	0.0	5.0	-0.3	5.0
2-3 (RIRM)	7.3	6.3	6.7	12	6-3 (RIRM)	1.6	2.3	0.1	2.8
2-a ( $I_{r0}$ )	—	—	—	3.2	6-a ( $I_{r0}$ )	—	—	—	1.0
2-a (RIRM)	-1.9	0.5	0.0	2.0	6-a (RIRM)	-0.8	0.1	-0.2	0.8
<i>Hexagonal pyrrhotite</i>					6-b ( $I_{r0}$ )	—	—	—	1.0
3-1 ( $I_{r0}$ )	-2.7	88	9.0	89	6-b (RIRM)	-0.9	0.2	0.1	1.0
3-1 (RIRM)	2.2	87	8.1	87	<i>Bensour meteorite (Ni-Fe)</i>				
3-2 ( $I_{r0}$ )	-9.9	90	-0.7	91	7-1 ( $I_{r0}$ )	-0.2	16	-0.8	16
3-2 (RIRM)	-8.1	85	5.7	85	7-1 (RIRM)	0.7	2.7	-8.6	9.0
3-3 ( $I_{r0}$ )	-0.5	75	-13	76	7-2 ( $I_{r0}$ )	0.2	7.2	0.3	7.2
3-3 (RIRM)	-1.5	57	-8.8	57	7-2 (RIRM)	-0.1	2.8	0.1	2.8
3-a ( $I_{r0}$ )	—	—	—	38	7-3 ( $I_{r0}$ )	-0.1	4.4	-0.3	4.4
3-a (RIRM)	-19	24	-13	33	7-3 (RIRM)	-0.4	3.5	0.6	3.6
3-b ( $I_{r0}$ )	—	—	—	50	7-a ( $I_{r0}$ )	—	—	—	5.7
3-b (RIRM)	-18	25	-26	40	7-a (RIRM)	-0.7	23	-2.2	23
<i>Monoclinic pyrrhotite 1</i>					<i>Magnetite-in-epoxy</i>				
4-1 ( $I_{r0}$ )	-0.3	2.4	0.4	2.5	8-1 ( $I_{r0}$ )	0.1	4.1	0.0	4.1
4-1 (RIRM)	1.8	2.2	0.5	2.9	8-1 (RIRM)	0.6	2.9	-0.4	3.0
4-2 ( $I_{r0}$ )	0.8	1.8	0.2	1.9	8-2 ( $I_{r0}$ )	0.0	1.5	0.1	1.5
4-2 (RIRM)	2.3	1.8	1.0	3.1	8-2 (RIRM)	0.5	1.1	-0.4	1.2
4-3 ( $I_{r0}$ )	0.1	2.0	-0.8	2.1	8-3 ( $I_{r0}$ )	0.1	3.1	0.1	3.1
4-3 (RIRM)	2.2	3.7	-1.9	4.7	8-3 (RIRM)	-0.1	1.0	0.0	1.1
4-a ( $I_{r0}$ )	—	—	—	1.7	8-a ( $I_{r0}$ )	—	—	—	0.2
4-a (RIRM)	-1.1	0.0	0.2	1.1	8-a (RIRM)	-0.1	0.0	0.0	0.1

\*\* Type of remanent magnetization  $I_r$ ;  $I_{r0}$ —pre-irradiation residual remanent magnetization remained after 120 mT AF demagnetization step, RIRM—radiation-induced remanent magnetization, measured after proton bombardment;  $I_{rx}$ ,  $I_{ry}$ ,  $I_{rz}$ , and  $I_r$  are  $x$ -,  $y$ -,  $z$ -components and total intensity of remanent magnetization, respectively (in % from post-irradiation SIRM,  $I_{rx}$  is positive while collinear with the direction of proton beam propagation.  $\{x, y, z\}$  is the coordinate system of 2G SQUID magnetometer.

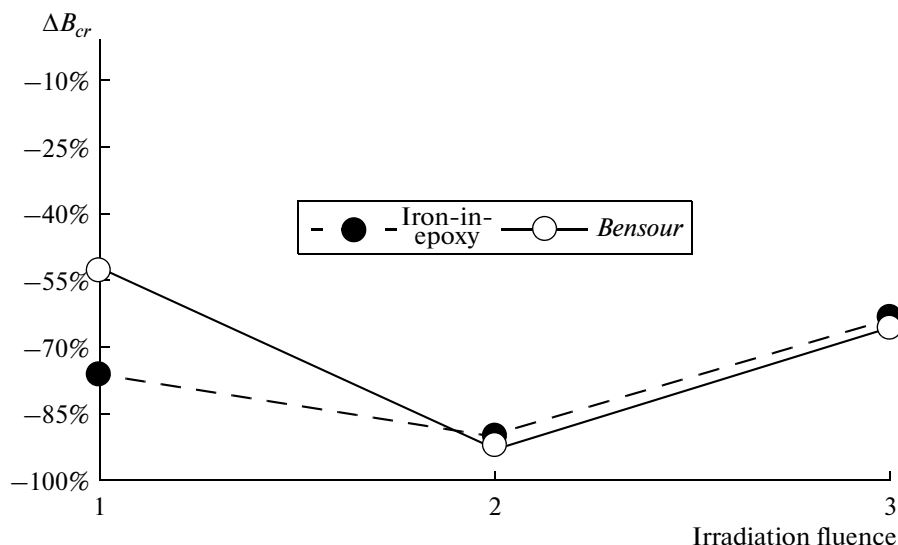


**Fig. 2.** Relative proton radiation-induced changes in coercivity of remanence  $B_{cr}$  for the samples of iron-in-epoxy and Bensour meteorite. Negative values reflect irradiation-induced magnetic softening (decrease in  $B_{cr}$ ).

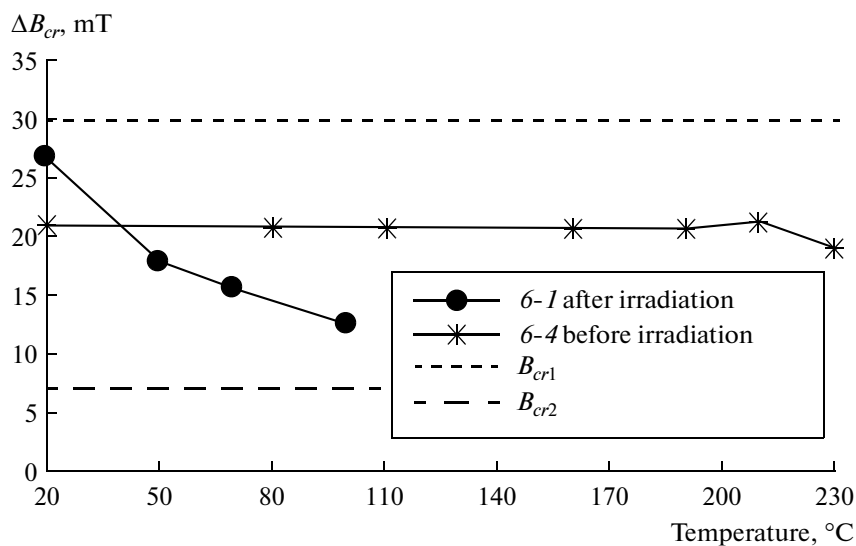


**Fig. 3.** Coercivity of remanence  $B_{cr}$  versus temperature for pristine (non-irradiated) iron-in-epoxy sample 6-4 and irradiated iron-in-epoxy sample 6-1. Annealing during 1–2 h was performed for the sample 6-4 at each temperature step. Sample 6-1 was annealed at each temperature step during 5 min.  $B_{cr1}$  and  $B_{cr2}$  are pre- and post-irradiation values, measured on the sample 6-1 before and shortly after proton bombardment experiment.

Hexagonal pyrrhotite samples are characterized by a decrease in  $B_{cr}$  (17%), minor changes in  $M_s$  ( $\leq 9\%$ ) and no changes in  $B_c$  ( $\leq 5\%$ ). We studied the magnetic properties of two pristine samples of hexagonal pyrrhotite (samples 3-4 and 3-5) upon heating. Contrary to what is observed after irradiation experiments, there is a dramatic decrease in  $B_{cr}$  and  $B_c$  observed for both hexagonal pyrrhotite samples upon heating (Table 4, Fig. 4). At the same time there is a significant post-

heating increase in  $M_{rs}$  and  $M_s$ , which is likely due to a creation of metastable ferrimagnetic grains. Other heating-induced changes are summarized in Table 4. All post-irradiation  $B_c$  and  $B_{cr}$  values are superior to the corresponding pre-heating and post-heating values for 3-4 and 3-5. So, as for other samples, radiation-induced changes in hexagonal pyrrhotite are not due to possible radiation-associated heating neither.

**Table 4.** Temperature effect on the magnetic properties of hexagonal pyrrhotite

Sample ID	$T$	$B_{cr}$	$B_c$	$B_{cr}/B_c$	$M_s$	$M_{rs}/M_s$
3-4 ( $m = 36.5$ mg)	20	242	120	2.0	4.4	0.39
	80	243	117	2.1	4.3	0.42
	110	220	109	2.0	4.4	0.37
	160	208	127	1.6	5.4	0.41
	190	170	108	1.6	9.3	0.41
	210	108	74	1.5	8.6	0.44
	230	25	17	1.5	47.8	0.24
3-5 ( $m = 21.7$ mg)	20	215	105	2.1	2.3	0.44
	80	207	—	—	—	—
	110	192	96	2.0	3.2	0.37
	160	185	108	1.7	4.4	0.35
	190	156	95	1.6	6.4	0.37

3-4 and 3-5 are two samples of pristine (non-irradiated) hexagonal pyrrhotite.  $m$  is mass;  $T$  is temperature (in °C);  $B_c$  and  $B_{cr}$  are coercivity and coercivity of remanence (in mT), respectively;  $M_s$  and  $M_{rs}$  are induced saturation magnetization and saturation remanent magnetization (in Am<sup>2</sup>), respectively. Annealing at each temperature step lasted 1–2 hours.

Contrary to the above-discussed cases, two magnetite-bearing samples (1-1 and 8-3) show a post-irradiation increase in  $B_{cr}$ . It is not consistent with the observed decrease in  $B_{cr}$  for the other samples of the same type (1-3, 8-2) nor with the corresponding  $\phi$ .

To evaluate the possibility of magnetic after-effect (Néel, 1952) on irradiated samples and possible changes of the magnetic properties with time after the irradiation, we remeasured  $B_{cr}$  of the iron-in-epoxy sample 6-1 after 24 months of storage in the Earth's magnetic field at room temperature. We observed a significant increase in  $B_{cr}$  compared with initial post-irradiation value. The sample almost returned to its pre-irradiation state within at most two years of relaxation. This may be explained by a diffusion after-effect mechanism (Néel, 1952), when lattice atoms displaced by the proton bombardment partially return to their initial lattice positions. This relaxation of crystalline point defects with time would erase the proton radiation-induced amorphization of iron. It is noteworthy that the irradiated iron sample became more sensitive to heating than the non-irradiated iron since heating up to 100°C (with 5-min annealing at each temperature step) decreased  $B_{cr}$  from 27 to 13 mT (Fig. 3).

We did not observe any changes in the frequency dependence of magnetic susceptibility after irradiation, which exclude that significant amount of superparamagnetic particles were formed during irradiation.

**4.1.3. Radiation-induced magnetization and demagnetization of samples.** Contrary to Rowe [1978], we observed significant changes in magnetic remanence of irradiated samples (Table 3, Figs. 5, 6). Some samples were demagnetized (hexagonal pyrrhotite, Bensour, magnetite-in-epoxy), others acquired remanent magnetization (monoclinic pyrrhotite, basalt, microdiorite). The fact that not all samples acquired remanent magnetization excludes the possibility of magnetic contamination (by manipulation with or vicinity to magnetic objects) during the experiments.

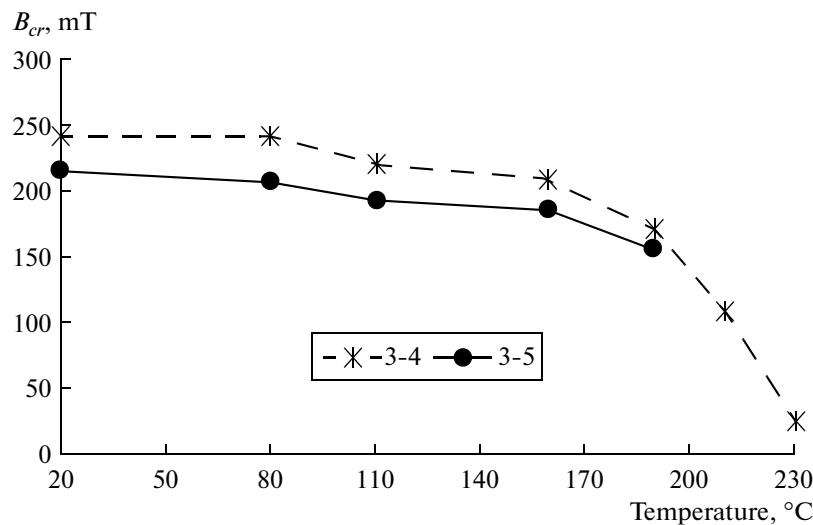


**Fig. 4.** Coercivity of remanence  $B_{cr}$  versus temperature for pristine (non-irradiated) massive samples of hexagonal pyrrhotite 3-4 and 3-5. There was 1–2 h annealing performed at each temperature step.

Therefore, the observed acquired remanence is likely linked to irradiation and is called RIRM in the following.

In most cases, RIRM was acquired perpendicular to the sample surface (further  $y-z$  plane), i.e., collinear to the direction of the proton beam propagation (further  $+x$ ). Therefore, in order to isolate proton-radiation induced acquisition of remanence and demagnetization of residual pre-irradiation remanence (i.e., magnetization along  $y$ -direction, remained after demagnetization of SIRM by alternating magnetic field of 120 mT), we plotted separately  $x$ -component and “in-plane”-component (i.e.,  $y-z$ ) of  $I_{r0}$  and RIRM (Fig. 5 and Fig. 6, respectively). Most samples show a significant magnetization acquisition collinear to the direction of the proton beam propagation and demagnetization or no changes of  $y-z$  component (regardless of overall magnetizing or demagnetizing effect). In case of increase of  $y-z$  component, it is minor if compared to  $x$ -component (<30% of  $x$ -component). The only exception is basaltic samples. So, in some cases (e.g., 7-1, 8-1, 8-2) we observe an acquisition of remanence along proton beam propagation direction (increase in  $x$ -component) in spite of overall demagnetizing effect found for total remanence.

Different magnetic mineralogies are characterized by a different response to proton bombardment. Also, there is no clear relation between irradiation dose and the intensity of RIRM. Examples of AF demagnetization curves of pre- and post-irradiation SIRM and RIRM as well as the corresponding Zijderveld orthogonal projection diagrams are given in Fig. 7a–7e. RIRM clearly affects only the low coercivity grains with MDFs in the 4 to 9 mT range. One may wonder whether the capacity of RIRM acquisition is related to the magnetic hardness of the samples. We do not observe such a correlation.

Rowe [1978] irradiated samples previously demagnetized by 80 mT AF (e.g., magnetite-in-epoxy, natural basaltic rock sample...) with 35 MeV protons, but did not observe any changes in remanent magnetization. The non-confirmation by Rowe [1978] of attempted RIRM might come from different samples or different proton energy range used in his experiments and is unlikely to be attributed to the low sensitivity of the magnetometer used in his study ( $\sim 10^{-9}$  Am<sup>2</sup>/g).

At the current stage of work the physical mechanism behind RIRM acquisition is still unclear and should be subject of future modeling. However, we can rule out acquisition of RIRM in the magnetic field generated by the proton beam due to the geometry of proton beam. Indeed, in our experiments proton beam (few mm in diameter) was swiping the irradiation surface (exposition window) with certain horizontal and vertical frequencies rather than being static and focused on one spot. The field generated by a fixed

proton beam would have been too low ( $\sim 0.4$  nT for 2  $\mu$ A current) to induce any significant remanence.

#### 4.2. Irradiation by Lead Ions

As in case of proton-irradiation with  $\phi_3$ , all samples embedded in epoxy or epoxy supports directly exposed to radiations showed a drastic change in color. Sadykov et al. [2011] reported a decrease in degree of order of Kapton polymer, bombarded with Pb ions, as a result of chain scission reactions. This mechanism is able to cause darkening of epoxy as well. As discussed above (see 4.1.1), because epoxy was not destroyed during irradiation, the maximum temperature was below 230°C. Total energy of the lead ions was 1 GeV (i.e.,  $\sim 5$  MeV/nucleon) and the maximum penetration depth did not exceed 200  $\mu$ m. This incident energy is much lower than the one currently observed for ions penetrating the solar cavity (GeV/nucleon).

**4.2.1. Radiation-induced changes in bulk magnetic properties of samples.** Some significant changes were observed in the bulk magnetic properties of lead-ion-irradiated samples (see Table 2). Contrary to proton-irradiation experiments, some changes in  $\chi_0$  (both increase and decrease) were observed: increase of 6 to 19% for all pyrrhotite-bearing samples, and decrease of 6 to 29% for magnetite and Ti-magnetite bearing samples. No or negligibly small changes in  $\chi_0$  are observed for iron and Bensour meteorite samples.

A decrease in  $B_{cr}$  (up to 58%) is observed for iron-bearing samples apart for the sample 6-b, which underwent partial mechanical destruction upon irradiation and this result may not be reliable. The effect of magnetic softening is accompanied by increase in SIRM (14–37%). Changes in the corresponding  $MDF_i$  values are minor (with exception of the sample 7-a, for which a 15% decrease is observed after ion bombardment).

Contrary to proton-irradiation experiments, there is an increase in  $M_s$  observed for both iron samples. Samples of monoclinic pyrrhotite do not demonstrate any significant changes apart for a slight decrease in SIRM. The samples of hexagonal pyrrhotite, for which only half of each sample was irradiated due to narrow exposition window, are characterized by decrease in  $B_c$  (12 and 25%) but negligible changes in  $M_s$ . A decrease in  $B_c$  is observed for the samples 3-4 and 3-5 during heating experiments (see Table 4). However, heating experiments resulted in a simultaneous increase in  $M_s$  and dramatic decrease in  $B_{cr}$ , which is not observed for lead-ion-irradiated samples.

Contrary to iron-bearing samples, both magnetite-bearing samples show a magnetic hardening ( $\sim 20\%$  increase in  $B_{cr}$ ), accompanied by an increase in  $B_c$  (11 to 25%) and 8% increase (1-a) and 16% decrease (8-a) in SIRM. It is consistent with an increase in  $MDF_i$  (4–9%). The effect of magnetic hardening had already been observed on the same samples (1-1, 8-3) after proton bombardment. The basalt sample (2-a) did not

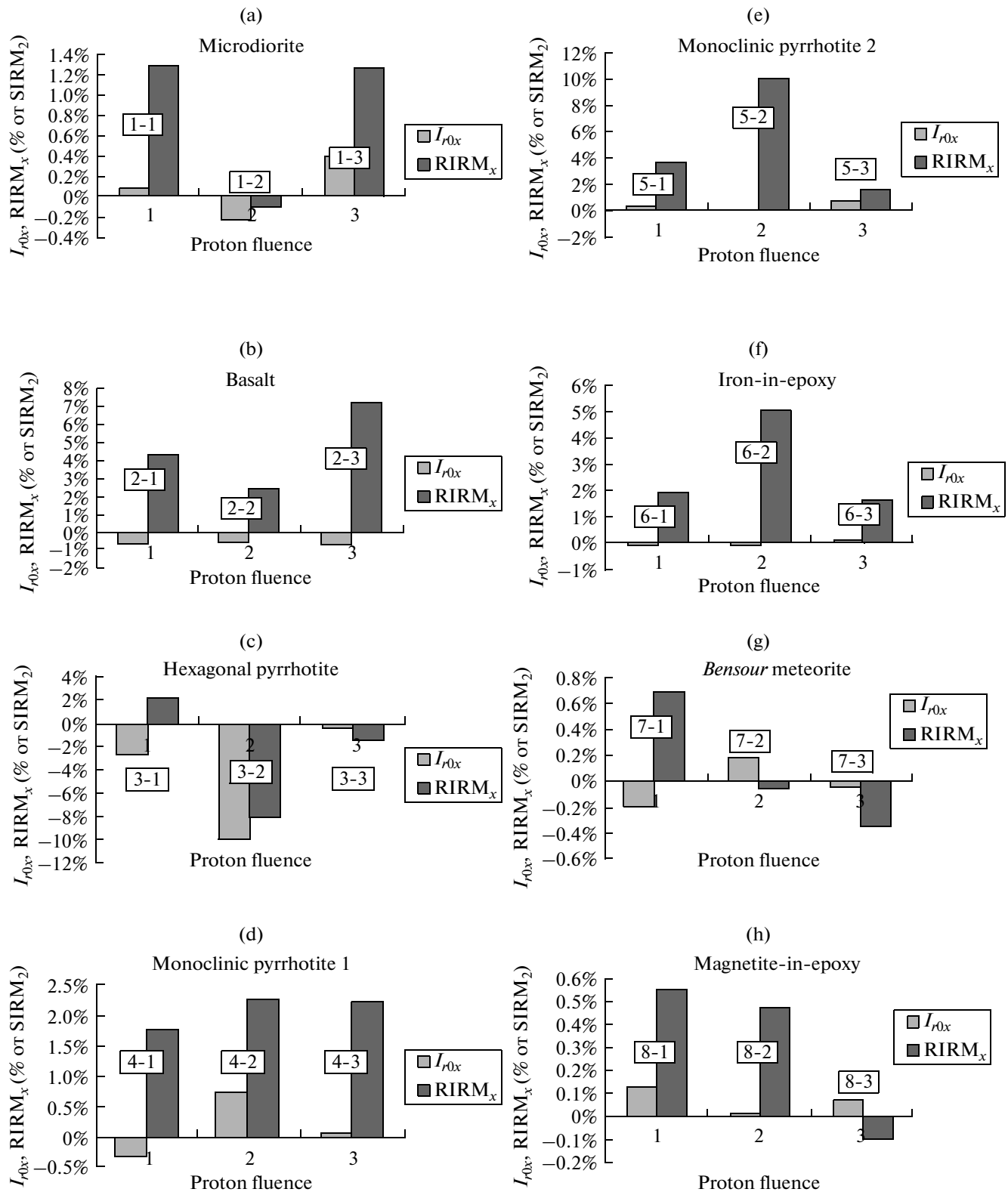


**Fig. 5.** Histograms of  $x$ -components of pre-irradiation ( $I_{r0x}$ ) and post-irradiation remanent magnetization ( $RIRM_x$ ) (in % from post-irradiation saturation isothermal remanent magnetization  $SIRM_2$ ) versus minimum, medium and maximum total irradiation fluences  $\phi_1$ ,  $\phi_2$  and  $\phi_3$ , respectively. (a) microdiorite; (b) basalt; (c) hexagonal pyrrhotite; (d) monoclinic pyrrhotite 1; (e) monoclinic pyrrhotite 2; (f) iron-in-epoxy; (g) Boursour meteorite; (h) magnetite-in-epoxy. For each double column, left and right columns indicate pre- and post-irradiation remanence, respectively.

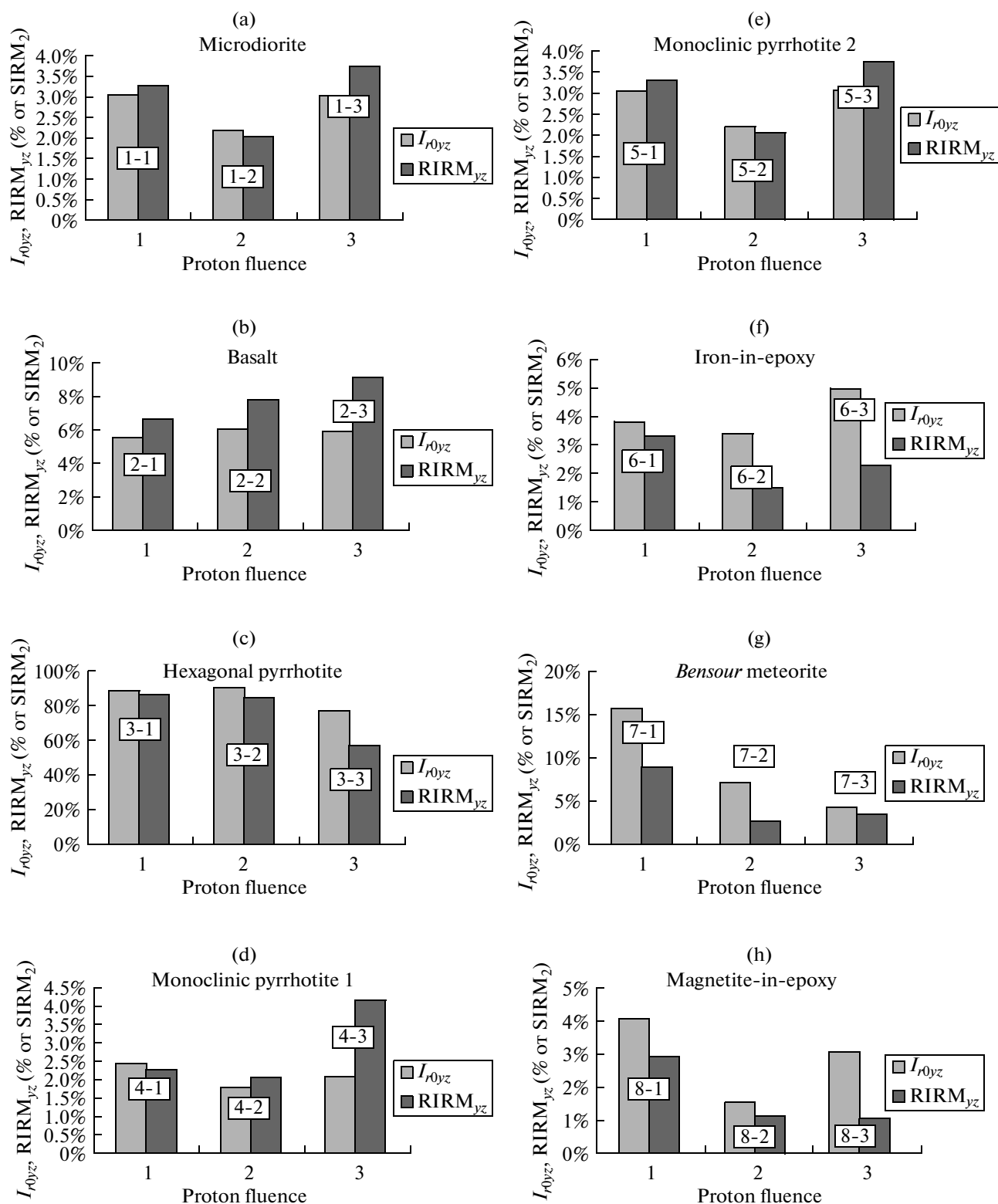


**Fig. 6.** Histograms of “in-plane”-components (i.e.,  $y-z$ ) of pre-irradiation ( $I_{r0yz}$ ) and post-irradiation remanent magnetization ( $RIRM_{yz}$ ) (in % from post-irradiation saturation isothermal remanent magnetization  $SIRM$ ) versus minimum, medium and maximum total irradiation fluences  $\phi_1$ ,  $\phi_2$  and  $\phi_3$ , respectively. (a) microdiorite; (b) basalt; (c) hexagonal pyrrhotite; (d) monoclinic pyrrhotite 1; (e) monoclinic pyrrhotite 2; (f) iron-in-epoxy; (g) Bensour meteorite; (h) magnetite-in-epoxy. For each double column, left and right columns indicate pre- and post-irradiation remanence, respectively.

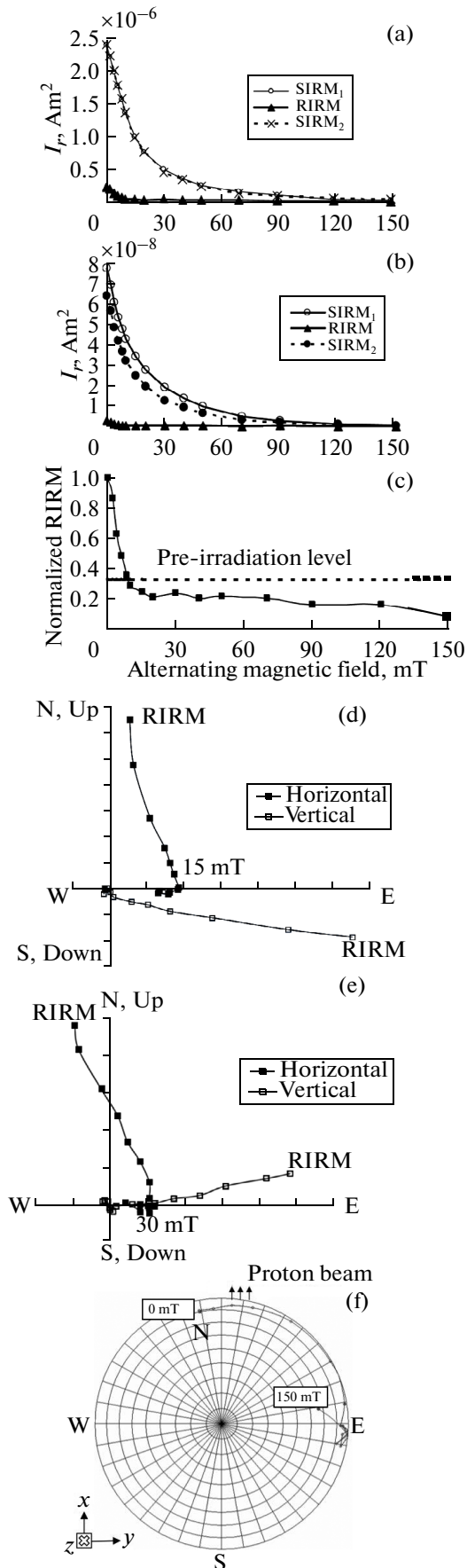


**Fig. 7.** (a) Pre- and post-irradiation saturation isothermal remanent magnetization SIRM and radiation isothermal remanent magnetization (RIRM) versus alternating magnetic field (AF) for the samples (a) 5-2 (monoclinic pyrrhotite 2), (b) iron-in-epoxy 6-2; (c) normalized RIRM versus AF for the sample 5-2; (d) Orthogonal vector projections (Zijderveld diagrams, EAST type) obtained at stepwise AF demagnetization up to 150 mT of RIRM for the sample (d) 6-2 and (e) 5-2; “horizontal” and “vertical” designate horizontal and vertical projections of magnetization. (f) Stereoplot obtained at step-wise demagnetization of RIRM for the sample 5-2 by alternating magnetic field up to 150 mT.  $\{x, y, z\}$  is the coordinate system of SQUID magnetometer. SIRM<sub>1</sub> is pre-irradiation SIRM and SIRM<sub>2</sub> is post-irradiation SIRM. N, E, W, S designate north, east, west and south, respectively.

show any significant radiation induced changes apart for 6% decrease in SIRM and  $MDF_i$ .

Lead-ion bombardment was not more effective in terms of changes of magnetic properties in the target materials, if compared with proton bombardment. It is consistent with comparable number of displaced atoms per incident particle in average collision cascade: 7.4 for protons (for both irradiation energies) against 8.5 for lead ions (see part 3.4).

**4.2.2. Radiation-induced remanent magnetization and demagnetization.** A significant remanent magnetization was acquired by some samples during irradiation by lead-ion. The lead-ion beam was perpendicular to sample surfaces, and the acquired magnetization is along this direction. Surprisingly,  $x$ -components of post-irradiation remanent magnetization ( $I_{rx}$ ) are collinear to the direction opposite to ion beam propagation for all samples.

Acquisition of RIRM occurred for two irradiated samples: microdiorite (1-a) and Bensour meteorite (7-a) acquired a RIRM with intensities of 4.8% (1-a) and 23% (7-a) of post-irradiation SIRM. Both samples are characterized by radiation-induced increase in SIRM (8% for 1-a and 37% for 7-a) and changes in  $B_{cr}$  (17% increase for 1-a and 6% decrease for 7-a), consistent with newly induced RIRM.  $MDF$  of RIRM is 4 mT for 1-a and 14 mT for 7-a. Overall demagnetizing effect of ion beam was observed for all the other samples (see Table 3).

**4.3. Irradiation by Argon Ions**

We investigated the magnetic properties of two meteorites previously irradiated by Vernazza et al. [2006]. The initial purpose of these  $Ar^{2+}$  irradiation experiments was to study the effect of space weathering at the surface of Vesta, it is detailed below.

Space rocks are darkened and reddened by the stream of ions from the Sun. But the surface of Vesta, the second-largest asteroid known in our Solar System, is surprisingly pristine. Argon ion irradiation experiments on an eucrite meteorite, which characterizes the surface of Vesta well, were carried out by Ver-

**Table 5.** Main rock magnetic properties of pristine and argon-ion-irradiated *Tatahouine* and *Bereba* meteorites

Sample ID	$\chi_0$	SIRM	$MDF_i$	$B_c$	$B_{cr}$	$B_{cr}/B_c$	$M_s$	$M_{rs}/M_s$
1 <i>Bereba (a)</i>	2.5	33	25	11	42	3.8	476.6	0.08
2 <i>Bereba (b)</i>	[2.5; 2.8]	[41; 45]	25	15	47	3.1	[329.5; 364.1]	0.10
3 <i>Tatahouine (a)</i>	0.5	0.6	14	$5 \pm 2$	$25 \pm 4$	[3.0; 9.7]	$157.2 \pm 134.4$	$0.02 \pm 0.01$
4 <i>Tatahouine (b)</i>	[2.1; 2.3]	[27; 30]	23	12	47	3.9	[303.7; 335.7]	0.07

$\chi_0$  is low-field magnetic susceptibility (in  $10^{-6} \text{ m}^3/\text{kg}$ ); SIRM is 3 T isothermal remanent magnetization (in  $\text{mA m}^2/\text{kg}$ ) measured with a 2G SQUID magnetometer;  $MDF_i$  is median destructive field of SIRM (in mT);  $B_c$  and  $B_{cr}$  are coercivity and coercivity of remanence (in mT), respectively;  $M_s$  and  $M_{rs}$  are induced saturation magnetization (in  $\text{mA m}^2/\text{kg}$ ) and saturation remanent magnetization, respectively. Each line 1, 2 and 4 correspond to one single meteorite pellet; line 3 regroups values from 9 bulk samples, so corresponding average values and standard deviations are indicated for each parameter ( $\chi_0$ , SIRM and  $MDF_i$  were measured only for one bulk sample). The margin of error for the estimation of mass of meteorite powder fraction in each of irradiated samples resulted in a range of mass-normalized  $\chi_0$ , SIRM and  $M_s$  values (line 2 and 4).

nazza et al. (2006) in order to simulate the SW irradiation on this asteroid. Argon ions were used for irradiation experiments rather than 1 keV protons—by far the most abundant in the SW—since their irradiation effect on the spectral properties of various silicates were previously shown to be much greater than with protons (Brunetto, Strazzulla, 2005). The Vernazza et al. (2006) study shows that Vesta should indeed be substantially more weathered than it appears. They suggest that the asteroid must have a magnetic field of at least  $0.2 \mu\text{T}$  at its surface, a few hundred times smaller than Earth's own magnetic field, which diverts the damaging ions. This hypothesis may explain why Vesta's surface looks fresh (unweathered).

As there were no magnetic measurements performed on irradiated meteorite samples prior to  $\text{Ar}^{2+}$  irradiation experiments, it is not possible to discuss here the possible effects on the remanent magnetization of argon-ion bombardment. The intrinsic magnetic properties of irradiated and pristine samples are given in Table 5. In order to check for the homogeneity of bulk magnetic properties of Tatahouine meteorite samples, we studied nine different pristine bulk Tatahouine samples with masses ranging from 79 to 631 mg. The results are rather homogeneous at this scale, with mean  $B_c = 5 \pm 2$  mT and  $B_{cr} = 25 \pm 4$  mT. This homogeneity allows comparison of the magnetic properties of pristine and irradiated samples even if they have not been measured on the same samples. These coercivity values are in agreement with the mean  $B_c$  value of  $4.0 \pm 3.0$  mT reported for seven diogenite falls (Gattacceca et al., 2008b), and with the mean  $B_{cr}$  value of  $53 \pm 19$  mT obtained from three diogenite falls (our unpublished data). But they are significantly smaller than that of the irradiated sample ( $B_c = 12$  mT,  $B_{cr} = 47$  mT). This magnetic hardening is observed for both Tatahouine and Bereba. It is consistent with neutron irradiation results (Butler and Cox, 1971; 1974), and is accompanied by simultaneous increase in SIRM and increase or no change in  $MDF_i$ , and thus is likely to be linked to the creation of point defects in crystalline structure of irradiated samples. There are no changes in  $\chi_0$  and a decrease in  $M_s$

observed for Bereba and slight increase in  $\chi_0$ , consistent with simultaneous increase in  $M_s$  observed for Tatahouine.

## 5. CONCLUSIONS

We performed particle radiation experiments using protons and ions in order to evaluate the possible effects of SEP and GCR on the magnetic properties of rocks and minerals. Both irradiation types lead to significant changes in the bulk magnetic properties (SIRM,  $M_s$  and  $B_{cr}$ ) of the studied samples. All  $\alpha\text{-Fe}_0\text{-}$  and FeNi-bearing samples showed a magnetic softening, with a strong decrease in  $B_{cr}$  (up to 93%). This effect is likely due to radiation-induced amorphization or atom disorder of metallic phases. Some magnetite-bearing samples demonstrate the opposite effect of magnetic hardening after proton and lead-ion bombardments. It is also the case for the samples of HED meteorites (Tatahouine and Bereba), irradiated by 400 keV  $\text{Ar}^{2+}$  ions.

Proton and lead-ion bombardments in the Earth-like magnetic field cause either demagnetization or magnetization of the target material, which is strongly dependent on the type of the magnetic mineralogy involved and, in some cases, on the type of ionizing radiation.

In case of magnetization, we observe a formation of so-called radiation-induced remanent magnetization (RIRM). This new type of remanence is characterized by low values of median destructive field (MDF): its intensity may be dependent on irradiation dose and magnetic mineralogy. The most effective RIRM production was found on Ti-magnetite-bearing rock samples as well as monoclinic pyrrhotite and iron-in-epoxy.

All together these results suggest that the combined effect of SEP (with penetration capacity up to hundreds  $\mu\text{m}$ ) and GCR radiations on the magnetic properties of extraterrestrial materials are to be considered for micrometeorites, meteoritic breccias and regolith as well as any surface material of solid Solar System bodies. Traces of SW-associated irradiation effects are

unlikely to be detectable in meteorites as SW protons penetration is limited to nm range and this irradiated thin crust disappear due to ablation of meteoroid in the terrestrial atmosphere.

Space radiations may result in the magnetic softening of metallic iron phases and magnetic hardening of magnetite-bearing materials and likely no changes in the magnetic hardness of pyrrhotite phases.

Additional irradiation experiments are needed to constrain the properties of RIRM (such as intensity and stability to thermal treatment). In particular, in order to understand if RIRM may account for NRM of some meteorites and lunar ground, it is necessary to find out if RIRM intensity depends on the strength and direction of the ambient magnetic field present during irradiation event, or if it can be produced in sub-null magnetic field.

#### ACKNOWLEDGMENTS

Authors are grateful to M. Fuller (University of Hawaii at Manoa), R.A. Sadykov (INR RAS, Russia), D. Fulvio (Laboratory for Atomic and Surface Physics, University of Virginia, USA) for helpful discussions. We thank B. Zanda and M. Gounelle from MNHN (Paris, France) to have provided bulk samples of Tatahouine meteorite used in this work.

This work was funded by the Agence Nationale de la Recherche (project ANR-09-BLAN-436 0042) and is performed according to the Russian Government Program of Competitive Growth of Kazan Federal University.

#### REFERENCES

- Alexeev, V.A., Meteorite ablation evaluated from data on the distribution of cosmogenic neon isotopes, *Solar System Res.*, 2003, vol. 37, no. 3, pp. 207–217.
- Alexeev, V.A., Meteorite ablation evaluated from the data on the density of cosmic ray tracks, *Solar System Res.*, 2004, vol. 38, no. 3, pp. 194–202.
- Bernas, H., Chaumont, J., Cottureau, E., Moroy, G., Clerc, C., Kaitasov, O., Ledu, D., and Salomé, M., Progress report on ARAMIS, the 2 MV tandem at Orsay, *Nucl. Instr. Meth. Phys. Res. B*, 1992, vol. 62, pp. 416–420.
- Binzel, R.P. and Xu, S., Chips off to asteroid 4 Vesta: evidence for the parent body of basaltic achondrite meteorites, *Science*, 1993, vol. 260, pp. 186–191.
- Bischoff, A., Scott, E.R.D., Metzler, K., and Goodrich, C.A., *Nature and Origins of Meteoritic Breccias. Meteoritics and the Early Solar System II*, Lauretta, D.S. and McSween, H.Y., Eds., 2006, pp. 679–712.
- Bronshthen, V.A., *Physics of Meteoric Phenomena*, Dordrecht, Holland: D. Reidel Publishing Company, 1983.
- Brunetto, R. and Strazzulla, G., Elastic collisions in ion irradiation experiments: A mechanism for space weathering of silicates, *Icarus*, 2005, vol. 179, pp. 265–273.
- Butler, R.F. and Cox, A.V., A mechanism for producing magnetic Remanence in meteorites and Lunar samples by cosmic-ray exposure, *Science*, 1971, vol. 172, pp. 939–941.
- Butler, R.F. and Cox, A.V., The effect of neutron irradiation on remanent magnetization of multidomain iron and kamacite, *J. Geomag. Geoelectr.*, 1974, vol. 26, pp. 55–71.
- Carpenter, R.H., Pyrrhotite isograd in SE Tennessee and SW North Carolina, *Geol. Soc. Am. Bull.*, 1974, vol. 85, pp. 451–456.
- Ceplecha, Z., Borovičhka, J., Elford, W.G., ReVelle, D.O., Hawkes, R.L., Porubčan, V., and Šimek, M., Meteor phenomena and bodies, *Space Sci. Rev.*, 1998, vol. 84, nos. 3–4, pp. 327–471.
- Consolmagno, G.J. and Drake, M.J., Composition and evolution of the eucrite parent body: evidence from rare earth elements, *Geochim. Cosmochim. Acta*, 1977, vol. 41, pp. 1271–1282.
- Dekkers, M.J., Magnetic properties of natural pyrrhotite part I: Behavior of initial susceptibility and saturation magnetization related parameters in a grain size dependent framework, *Phys. Earth Planet. Inter.*, 1988, vol. 52, pp. 376–393.
- Diehl, R., Kallenbach, R., Parizot, E., and Von Steiger, R., The astrophysics of Galactic cosmic rays, *Space Sci. Rev.*, 2001, vol. 99, pp. 3–11, doi:10.1023/A:1013882424934.
- Dienes, G.J. and Vineyard, G.H., *Radiation Effects in Solids*, New York: Interscience, 1957.
- Dubinin, S.F., Parkhomenko, V.D., Teploukhov, S.G., and Goshchitskii, B.N., Amorphization of solids by fast neutrons, *Phys. Sol. Stat.*, 1998, vol. 40, no. 9, pp. 1436–1440.
- Eugster, O., Herzog, G.F., Marti, K., and Caffee, M.W., *Irradiation Records, Cosmic-Ray Exposure Ages, and Transfer Time of Meteorites. Meteoritics and the Early Solar System II*, Lauretta, D.S. and McSween, H.Y., Eds., 2006, pp. 829–851.
- Feigelson, E.D., Garmire, G.P., and Pravdo, S.H., Magnetic flaring in the pre-main-sequence Sun and implications for the early Solar System, *Astrophys. J.*, 2002, vol. 572, pp. 335–349.
- Fulvio, D., Brunetto, R., Vernazza, P., and Strazzulla, G., Space weathering of Vesta and V-type asteroids: new irradiation experiments on HED meteorites, *Astron. Astrophys.*, 2012, vol. 537, pp. L11 (1–5), doi: 10.1051/0004-6361/201118486.
- Gattacceca, J., Rochette, P., and Bourot-Denise, M., Magnetic properties of a freshly fallen LL ordinary chondrite: the Bensour meteorite, *Phys. Earth Planet. Inter.*, 2003, vol. 140, pp. 343–358.
- Gattacceca, J., Lamali, A., Rochette, P., Boustie, M., and Berthe, L., The effect of explosive-driven shocks on the natural remanent magnetization and the magnetic properties of rocks, *Phys. Earth Planet. Inter.*, 2007, vol. 162, pp. 85–98.
- Gattacceca, J., Berthe, L., Boustie, M., Vadeboin, F., Rochette, P., and De Resseguier, T., On the efficiency of shock magnetization processes, *Phys. Earth Planet. Inter.*, 2008a, vol. 166, pp. 1–10.
- Gattacceca, J., Rochette, P., Gounelle, M., and Van Ginneken, M., Magnetic anisotropy of HED and Martian meteorites and implications for the crust of Vesta and Mars, *Earth Planet. Sci. Lett.*, 2008b, vol. 270, pp. 280–289, doi: 10.1016/j.epsl.2008.03.047.
- Gordon, G.Ya., *Stabilization of Synthetic Polymers*, Moscow: Goskhimizdat, 1963 [in Russian].

- Goswami, J.N., Marhas, K.K., and Sahijpal, S., Did Solar energetic particles produce the short-lived nuclides present in the early Solar System?, *Astrophys. J.*, 2001, vol. 549, pp. 1151–1159, doi:10.1086/319434.
- Hapke, B., Space Weathering from Mercury to the asteroid belt, *J. Geophys. Res.*, 2001, vol. 106 (E5), pp. 10039–10073, doi: 10.1029/2000JE001338.
- Heiken, G., Vaniman, D., and French, B.M., *Lunar Sourcebook A User's Guide to the Moon*, Cambridge: Cambridge University Press, 1991.
- Herzog, G.F., *Cosmic-ray Exposure Ages of Meteorites. Treatise on Geochemistry, Vol. 1: Meteorites, Comets, and Planets*, Davis, A.M., Ed., 2005, pp. 347–380.
- Holbert, K.E., Radiation effects and damage, *Dr. Holbert's Course "EEE 598—Radiation Effects"*, School of Electrical, Computer and Energy Engineering, Arizona State University. <http://holbert.faculty.asu.edu/eee560/eee560.html>
- Kapitonov, I.M., *Introduction to Nuclear and Particle Physics*, Moscow: Editorial URSS, 2002 [in Russian].
- Kircher, J.F. and Bowman, R.E., *Effects of Radiation on Materials and Components*, New York: Reinhold Publishing, 1964.
- Koptelov, E.A., Latysheva, L.N., Sobolevsky, N.M., and Mustafin, E., Review of experimental and theoretical works on irradiation of a polyimide by protons and ions, *Preprint Institute for Nuclear Research RAS-1197/2008*, 2008 [in Russian].
- Lee, T., Shu, F.H., Shang, H., Glassgold, A.E., and Rehm, K.E., Protostellar cosmic rays and extinct radioactivities in meteorites, *Astrophys. J.*, 1998, vol. 506, pp. 898–912.
- Néel, L., Théorie du traînage magnétique de diffusion, *J. Phys. Rad.*, 1952, vol. 13, pp. 249–263.
- Néel, L., Pauleve, J., Pauthenet, R., Laugier, J., and Dautreppe, A., Magnetic properties of an iron-nickel single crystal ordered by neutron bombardment, *J. Applied Geophys.*, 1964, vol. 35, pp. 873–876.
- Pieters, C.M., Taylor, L.A., Noble, S.K., Keller, L.P., Hapke, B., Morris, R.V., Allen, C.C., McKay, D.S., and Wentworth, S., Space weathering on airless bodies: resolving a mystery with lunar samples, *Meteorit. Planet. Sci.*, 2000, vol. 35, pp. 1101–1107.
- Preibisch, T. and Feigelson, E.D., The evolution of X-ray emission in young stars, *Astrophys. J. Suppl. Ser.*, 2005, vol. 160, pp. 390–400.
- Rochette, P., Fillion, G., Ballou, R., Brunet, F., Ouladdiaf, B., and Hood, L., High pressure magnetic transition in pyrrhotite and impact demagnetization on Mars, *Geophys. Res. Lett.*, 2003a, vol. 30, p. 1683, doi:10.1029/2003GL017359.
- Rochette, P., Sagnotti, L., Bourot-Denise, M., Consolmagno, G., Folco, L., Gattacceca, J., Osete, M.L., and Pesonen, L., Magnetic Classification of stony meteorites: 1. Ordinary chondrites, *Meteorit. Planet. Sci.*, 2003b, vol. 38, pp. 251–258.
- Rochette, P., Gattacceca, J., Bonal, L., Bourot-Denise, M., Chevrier, V., Clerc, J.-P., Consolmagno, G., Folco, L., Gounelle, M., Kohout, T., Pesonen, L., Quirico, E., Sagnotti, L., and Skripnik, A., Magnetic classification of stony meteorites: 2. Non-ordinary chondrites, *Meteorit. Planet. Sci.*, 2008, vol. 43, pp. 959–980, doi:10.1111/j.1945-5100.2008.tb01092.x.
- Rochette, P., Weiss, B.P., and Gattacceca, J., Magnetism of extraterrestrial materials, *Elements*, 2009a, vol. 5, pp. 229–234.
- Rochette, P., Gattacceca, J., Bourot-Denise, M., Consolmagno, G., Folco, L., Kohout, T., Pesonen, L., and Sagnotti, L., Magnetic classification of stony meteorites: 3. Achondrites, *Meteorit. Planet. Sci.*, 2009b, vol. 44, pp. 405–427, doi:10.1111/j.1945-5100.2009.tb00741.x.
- Rowe, M.W., Attempted proton-irradiation induced magnetization, *Geochem. J.*, 1978, vol. 12, pp. 195–197.
- Sadykov, R.A., Shiryayev, A.A., Gavriluk, A.G., Seidl, T., Mustafin, E., Sadykova, I.R., and Koptelov, E.A., Nanostructure of Pb ion irradiate Kapton (polyimide), *Book of Abstracts of the Rusnanotech—Nanotechnology International Forum 2011*, Moscow, 2011.
- Sears, D.W., *The origin of Chondrules and Chondrites*, Cambridge: Cambridge Univ. Press, 2004.
- Serruys, Y., Ruault, M.-O., Trocellier, P., Henry, S., Kaitasov, O., and Trouslard, Ph., Multiple ion beam irradiation and implantation: JANNuS project, *Nucl. Instr. Meth. Phys. Res. B*, 2005, vol. 240, pp. 124–127.
- Strazzulla, G., Dotto, E., Binzel, R., Brunetto, R., Barucci, M.A., Blanco, A., and Orofino, V., Spectral alteration of the Meteorite Epinal (H5) induced by heavy ion irradiation: A simulation of space weathering effects on near-Earth asteroids, *Icarus*, 2005, vol. 174, pp. 31–35.
- Sugiura, N. and Strangway, D.W., *Magnetic Studies of Meteorites. Meteorites and the Early Solar System*, Kerridge, J.F. and Mathews, M.S., Eds., 1988, pp. 595–615.
- Tetelbaum, D.I. and Mendeleva, Yu.A., A mechanical model of amorphization under ion bombardment, *Phys. Sol. Stat.*, 2004, vol. 46, no. 11, pp. 2026–2029.
- Vernazza, P., Brunetto, R., Strazzulla, G., Fulchignoni, M., Rochette, P., Meyer-Vernet, N., and Zouganelis, I., Asteroid colors: a novel tool for magnetic field detection? The case of Vesta, *Astron. Astrophys.*, 2006, vol. 451, pp. L43–L46, doi: 10.1051/0004-6361:20065176.
- Vernazza, P., Binzel, R.P., Thomas, C.A., DeMeo, F.E., Bus, S.J., Rivkin, A.S., and Tokunaga, A.T., Compositional differences between meteorites and near-Earth asteroids, *Nature*, 2008, vol. 454, pp. 858–860, doi: 10.1038/nature07154.
- Vernazza, P., Binzel, R.P., Rossi, A., Fulchignoni, M., and Birlan, M., Solar wind as the origin of rapid reddening of asteroid surfaces, *Nature*, 2009, vol. 458, pp. 993–995, doi: 10.1038/nature07956.
- Weiss, B.P., Gattacceca, J., Stanley, S., Rochette, P., and Christensen, U.R., Paleomagnetic records of meteorites and early Planetesimal differentiation, *Space Science Reviews*, 2010, vol. 152, pp. 341–390.
- Wolk, S.J., Harnden, F.R.Jr., Flaccomio, E., Micela, G., Favata, F., Shang, H., and Feigelson, E.D., Stellar activity on the young Suns of Orion: COUP observations of K5-7 Pre-Main-Sequence Stars, *Astrophys. J. Suppl. Ser.*, 2005, vol. 160, no. 2, pp. 423–449, doi:10.1086/432099.
- Ziegler, J.F., SRIM-2003, *Nucl. Instr. Meth. Phys. Res. Sec. B*, 2004, vol. 219–220, pp. 1027–1036, doi:10.1016/j.nimb.2004.01.208.